HHS Public Access

Author manuscript

J Mater Sci Mater Med. Author manuscript; available in PMC 2018 June 11.

Published in final edited form as:

J Mater Sci Mater Med. 2013 August ; 24(8): 1963–1975. doi:10.1007/s10856-013-4945-y.

Porous CaP/silk composite scaffolds to repair femur defects in an osteoporotic model

Ning Cheng,
The State Key Laboratory Breeding Base of Basic Science of Stomatology (Hubei-MOST) & Key Laboratory of Oral Biomedicine Ministry of Education, School & Hospital of Stomatology, Wuhan University, 237 Luoyu Road, Wuhan 430079, People's Republic of China

Jing Dai,
The State Key Laboratory Breeding Base of Basic Science of Stomatology (Hubei-MOST) & Key Laboratory of Oral Biomedicine Ministry of Education, School & Hospital of Stomatology, Wuhan University, 237 Luoyu Road, Wuhan 430079, People's Republic of China

Xiangrong Cheng,
The State Key Laboratory Breeding Base of Basic Science of Stomatology (Hubei-MOST) & Key Laboratory of Oral Biomedicine Ministry of Education, School & Hospital of Stomatology, Wuhan University, 237 Luoyu Road, Wuhan 430079, People's Republic of China

Shu'e Li,
The State Key Laboratory Breeding Base of Basic Science of Stomatology (Hubei-MOST) & Key Laboratory of Oral Biomedicine Ministry of Education, School & Hospital of Stomatology, Wuhan University, 237 Luoyu Road, Wuhan 430079, People's Republic of China

Richard J. Miron,
The State Key Laboratory Breeding Base of Basic Science of Stomatology (Hubei-MOST) & Key Laboratory of Oral Biomedicine Ministry of Education, School & Hospital of Stomatology, Wuhan University, 237 Luoyu Road, Wuhan 430079, People's Republic of China. Department of Periodontology, School of Dental Medicine, Freiburgstrasse 7, Postfach 64, 3010 Bern 10, Switzerland

Tao Wu,
The State Key Laboratory Breeding Base of Basic Science of Stomatology (Hubei-MOST) & Key Laboratory of Oral Biomedicine Ministry of Education, School & Hospital of Stomatology, Wuhan University, 237 Luoyu Road, Wuhan 430079, People's Republic of China

Wenli Chen,
The State Key Laboratory Breeding Base of Basic Science of Stomatology (Hubei-MOST) & Key Laboratory of Oral Biomedicine Ministry of Education, School & Hospital of Stomatology, Wuhan University, 237 Luoyu Road, Wuhan 430079, People's Republic of China

Yufeng Zhang, and

Correspondence to: Bin Shi.
Ning Cheng and Jing Dai contribute equally to the study.

The State Key Laboratory Breeding Base of Basic Science of Stomatology (Hubei-MOST) & Key Laboratory of Oral Biomedicine Ministry of Education, School & Hospital of Stomatology, Wuhan University, 237 Luoyu Road, Wuhan 430079, People's Republic of China

Bin Shi

The State Key Laboratory Breeding Base of Basic Science of Stomatology (Hubei-MOST) & Key Laboratory of Oral Biomedicine Ministry of Education, School & Hospital of Stomatology, Wuhan University, 237 Luoyu Road, Wuhan 430079, People's Republic of China

Abstract

The most common complication for patients with postmenopausal osteoporosis is bone-related defects and fractures. While routine medication has a high probability of undesirable side effects, new approaches have aimed to develop regeneration procedures that stimulate new bone formation while reversing bone loss. Recently, we have synthesized a new hybrid CaP/silk scaffold with a CaP-phase distribution and pore architecture better suited to facilitate cell differentiation and bone formation. The aim of the present study was to compare the involved remodeling process and therapeutic effect of porous CaP/silk composite scaffolds upon local implantation into osteoporotic defects. Wistar rats were used to induce postmenopausal osteoporotic model by bilateral ovariectomy. The pure silk and hybrid CaP/silk scaffolds were implanted into critical sized defects created in distal femoral epiphysis. After 14 and 28 days, the in vivo osteogenetic efficiency was evaluated by μCT analysis, hematoxylin and eosin staining, Safranin O staining, tartrate-resistant acid phosphatase staining, and immunohistochemical assessment. Animals with or without critical-sized defects were used as drill or blank controls, respectively. The osteoporotic defect model was well established with significantly decreased μCT parameters of BV/TV, Tb.N and increased Tb.Sp, porosity, combined with changes in histological observations. During the healing process, the critical-sized drill control defects failed to regenerate appreciable bone tissue, while more significantly increased bone formation and mineralization with dynamic scaffold degradation and decreased osteoclastic bone resorption could be detected within defects with hybrid CaP/silk scaffolds compared to pure silk scaffolds.

1 Introduction

Osteoporosis is a worldwide emerging healthcare issue and socioeconomic threat characterized by reduction in bone mass, poor bone strength and microarchitectural deterioration in trabecular and cortical skeleton, leading to a consequence risk in skeletal fragility and susceptibility to fractures. It is an age-related disease caused by the imbalance between osteoblastic bone formation and osteoclastic bone resorption commonly resulting from postmenopausal estrogen deficiency [1, 2]. Over 200 million people are estimated to be affected by osteoporosis worldwide [3], and approximately 50 % of 65-year-old postmenopausal white or Asian women will experience an osteoporotic fracture [4]. For decades, several studies have shown that defect healing in postmenopausal osteoporotic women are delayed, mainly due to the absence of estrogen associated with a rise in osteoclast number [2, 5–7]. Since osteoporosis-related fractures are commonly occurring in long bone sites under loading environment, mechanical interference may affect the healing process. At present, the two major pharmacological approaches for the treatment of

osteoporosis are anabolic agents such as parathyroid hormone (PTH) by stimulating bone formation and anti-resorptive agents including bisphosphonates, calcitonin, raloxifene, and estrogen which act by inhibiting bone resorption [8]. Although much emphasis has been given to the treatment of osteoporosis and fracture prevention by using the above mentioned agents, less investigation has been conducted on the therapeutic effect of local transplantation of biomaterial scaffolds during osteoporotic defect regeneration.

Silk is basically composed of fibrous polypeptide in β-sheet form, whose main component is glycine, alanine and sericin [9]. It can be naturally derived from insects and formed via genetic engineering or the modification of native silk fibroin sequence chemistries [10]. Considering the superior properties of lightweight, degradable, high tensile strength, tough, inexpensive and ease of processing[11], it provided new options to further expand the utilization of silk fibroin-based scaffolds for ligament, bone and cartilage tissue regeneration [9, 12]. Several properties including less toxic, non-inflammatory, non-immunogenic, biodegradable and bioresorbable were tested by both in vitro and in vivo studies [12–14]. Accordingly, they have been gaining widespread attention as controlled-release carriers or templates for cellular activities in bone tissue engineering, whereas the osteoconductivity of pure silk scaffold is inferior compared to ceramic scaffolds. In contrast, calcium phosphate (CaP) has been the most commonly used biocompatible bone substitute for both dental and orthopedic applications, due to its similar inorganic composition, structure and mechanical properties to the mineralized bone tissue [15, 16]. CaP exhibits a high protein binding strength, and the dissolution of inorganic ions is followed by the reprecipitation of mineralized phase between bone tissue and scaffolds, yielding enhanced bone–matrix interface strength [17, 18].

To find an optimal solution for further application, porous hybrid CaP/silk scaffolds were synthesized, yielding a composite with the superior osteoconductivity and osteoinductivity of CaP and the mechanical flexibility of natural polymers. In our previous study, CaP/silk powders were successfully incorporated into silk scaffold by freeze-drying method, resulting in a uniformly distributed CaP particle within 3D silk scaffolds without compromising the mechanical strength, and providing an appropriate environment for BMSCs attachment, proliferation and osteogenic differentiation [19]. Also, we found that 5 % (w/v) hybrid CaP/silk scaffolds can promote new bone formation in calvarial defect mice, indicating its excellence in initial bone healing. So far, the recent findings and comparative studies were given more emphasis on demonstrating the osteogenesity of CaP/silk scaffolds for in vitro assessment and in non-skeletal disease conditions, whereas no investigation has been conducted for their application in metabolic skeletal diseased models. Till now, this is the first report on transplanting hybrid CaP/silk scaffolds into osteoporotic critical sized femur defects, thus to study the involved bone remodeling process and to investigate their in vivo therapeutic effect. We hypothesize that incorporation of newly developed CaP/silk scaffolds will improve the speed and quality of new bone formation in osteoporotic defects by studying their implantation into femurs in ovariectomized rats.

2 Materials and methods

2.1 Fabrication of porous hybrid CaP/silk scaffolds

Silk fibroin was extracted from mulberry silk cocoons according to a previous report [20]. CaP/silk hybrid powders were synthesized using a co-precipitation method, which was described in detail in our previous study [19]. Porous 3D silk scaffolds containing CaP/silk hybrid powders were prepared using a freeze-drying method. 5 % (w/v) CaP/silk hybrid powder was added into 10 ml of 5 % (w/v) silk water solutions under stirring to form a uniform mixture, followed by shifting into plastic dishes at 4 °C for 30 min, and placing in a freezer at −35 °C overnight to induce phase separation. A solidified membrane was formed and maintained at −80 °C for 2 h and was freeze-dried for 48 h to remove the solidified solvent. Finally, the hybrid scaffolds were rinsed with 90 % (v/v) ethanol.

2.2 Animals and surgical protocols

Animal handling and surgical procedures were conducted according to the guidelines for animal care and use committee of Wuhan University, People's Republic of China, and approved by the Ethics Committee at the School of Dentistry, prior to the start of this experiment. All animals were kept at 20–25 °C under a 12-h light/dark cycle and allowed food and water ad libitum. All operations were carried out under sterile conditions with a gentle surgical technique. The surgeon was blinded to the treatment. A single intramuscular dose of penicillin 40,000 IU/ml was then administered postoperatively. No significant perioperation or postoperation fractures were produced.

2.2.1 Osteoporotic model—5-month-old mature female Wistar rats were used for this experiment. In order to induce an osteoporotic model, the rats were subjected to bilateral ovariectomy (OVX) or sham operation (Sham) at 3 months of age (weight 200 ± 10 g). After anesthetization by intraperitoneal injection of sodium pentobarbital (40 mg/kg body weight), a lumbar lateral incision was made around the midpoint between the lower margin of free ribs and iliac crest, where the ovary was located. A suture was placed around the ovarian artery and vein prior to the removal of ovary. To tightly close the incision, the muscles were repositioned in layers and sutured with resorbable suture, and the skin was closed with nylon 4-0 suture. Timing of surgery on Sham and OVX rats was illustrated in Fig. 1a. The body weight of both Sham and OVX rats was measured at the end of induction.

2.2.2 Femur defect model—After 2-month-induction, drilling of the femur was performed under general anaesthesia by intraperitoneal injection of sodium pentobarbital (40 mg/kg body weight). A linear skin incision of approximately 1 cm in the distal femoral epiphysis was made bilaterally and blunt dissection of the muscles was performed to expose the femoral condyle. Then, a 2.5-mm-diameter latero-lateral channel was created perpendicular to the shaft axis to destroy cancellous trabecular bone (Fig. 1b, c), by using a trephine bur at a slow speed irrigated under saline solution to avoid thermal necrosis. The drilled holes were rinsed by injection with saline solution in order to remove bone fragments from the cavity. Implant scaffolds were then gently placed to fill the drilled defects according to group allocation. Subsequently, the incision was closed as mentioned above.

Thereafter, the rats were divided into groups including Sham ($n = 3$), OVX ($n = 3$), OVX (blank control; $n = 6$), OVX + drilled defect (drill control; $n = 6$), OVX + pure silk ($n = 6$), OVX + 5 % hybrid CaP/silk ($n = 6$), respectively. The rats from Sham and OVX were considered as confirmation of the osteoporotic model after two-month-induction, and were sacrificed by cervical dislocation under sodium pentobarbital anesthesia following fasting overnight, so as to ensure their unconsciousness for euthanasia. All persons performing euthanasia are properly trained and supervised during animal experiment. At time points, 14 and 28 days after femur surgery, rats in the remaining four groups were sacrificed, accordingly. All femurs were removed and assigned to micro-computerized tomography (μCT) analysis and histological studies.

2.3 μCT analysis

The samples were fixed in 4 % paraformaldehyde for 24 h at room temperature. A μCT imaging system (μCT50, Scanco Medical, Basersdorf, Switzerland) was used: (i) to identify the establishment of the osteoporotic model with microarchitectural changes and (ii) to evaluate new bone formation within the defect region. All samples were placed in a custom-made holder to ensure that the long axis of the drilled channel was oriented perpendicular to the axis of X-ray beam. Scanning was performed at 55 kV and 114 μA with a thickness of 0.048 mm per slice in medium-resolution mode, 1,024 reconstruction matrix, and 200 ms integration time. These images and parameters were compared between two groups to confirm the osteoporotic model induced in rats. A Gaussian filter (sigma = 0.8 and support = 1) was used to remove noise. The mineralized bone tissue was differentially segmented to exclude the non-mineralized tissue with a fixed threshold (value = 190).

For conformation of the established osteoporotic model, a series of slices starting at a distance of 1 mm proximal from the end of the growth plate with a length of 2 mm were chosen for evaluation. For analysis of the bone regeneration process within the defect, the central region of the 2.5-mm-diameter defect was defined by drawing circular contour as area of measurement per slice, thus to obtain a consistent volume of interest (VOI) and to avoid including the native bone margins. After 3D reconstruction, the bone volume faction (BV/TV), trabecular number (Tb.N), trabecular thickness (Tb.Th) and trabecular separation (Tb.Sp) were automatically determined for identification of the osteoporotic model while bone volume faction (BV/TV) in defect regions were used to evaluate new bone formation, using a protocol provided by the manufacturer of the micro-CT scanner. The porosity (P) of bone was calculated as [21]:

$$P = 100\% - (BV/TV)$$

All digitalized data and 3D images were generated by the built-in software of the μCT.

2.4 Histological preparation and immunohistochemical studies

After μCT imaging, femoral condyles were decalcified in 10 % ethylene diamine tetraacetic acid (EDTA) for 2 weeks, changed twice per week, and then dehydrated in a series of graded concentration of ethanol from 70 to 100 %. To get a distinct view of the defect, the orientation and alignment of femurs were carefully considered during paraffin embedding.

Longitudinal serial sections, 4 mm thick, were cut and mounted on polylysine-coated microscope slides. For general histological studies, hematoxylin and eosin (H&E) staining, Safranin O staining (Sigma #S2255; Sigma-Aldrich, St. Louis, USA) and tartrate-resistant acid phosphatase (TRAP) staining (Sigma #387A; Sigma-Aldrich, St. Louis, USA.) were performed according to manufacturer's protocol.

For immunohistochemical assessment, the expression of type I collagen (COL1) and osteopontin (OPN) were detected according to the following procedure. Deparaffinised sections were washed with PBS, incubated with 0.3 % hydrogen perioxide for 20 min to block endogenous peroxidase activity, followed by incubation with 5 % bovine serum albumin (BSA). Then, sections were incubated with optimal concentrations of primary antibody for COL1 (1:100; Sigma-Aldrich, St. Louis, USA) and OPN (1:200; Biomedical Technologies, Stoughton, MA) overnight at 4 °C. After three washes with PBS, sections were incubated with biotinylated secondary antibody (Zhongshan Biotechnology Co., Ltd, China) for 20 min before incubation with horseradish peroxidase-conjugated avidin–biotin complex (ABC) (Zhongshan Biotechnology Co., Ltd, China) for another 20 min. Immunostaining was visualized after the addition of a buffered 3,3-diaminobenzidine tetrahydrochloride (DAB) (Zhongshan Biotechnology Co., Ltd, China) substrate. Sections were then counterstained with Harris's hematoxylin for 40 s each, in between 3 min rinses with running water. Subsequently, sections were dehydrated with ascending concentrations of ethanol solutions, cleared with xylene, and mounted with coverslips. Specimens were examined under a microscopic light by using an Olympus DP71 microscope (Olympus Co., Japan). To validate the results, each experiment was repeated at least three times.

Bone regeneration of these histological sections was scored on a semiquantitative scale by an individual blinded observer, using a modified scoring method similar to that described previously [22] (Table 1). By using Image J 1.44 software from the National Institute of Health (NIH, Bethesda, Maryland, USA), the fraction of scaffold remnants was calculated as previously described [23, 24]. The number of osteoclasts was counted under a light microscope (Olympus DP72; Olympus Co., Japan) as previously described [25]. Cells positively stained for TRAP containing more than three nuclei were defined as osteoclasts [26]. The bone histomorphometry and TRAP-positive multinuclear osteoclast measurements were performed on three consecutive sections of each specimen. From each section, three representative fields (1024 × 1536 pix) were identified (original magnification 10×) and averaged.

2.5 Statistical analysis

All statistical analysis was performed by using SPSS 17.0 software (SPSS, Chicago, IL). Data were expressed as mean ± standard deviation (SD) and were analyzed using one-way ANOVA and *t* test. For the bone regeneration score, the Kruskal–Wallis H test was used followed by Mann–Whitney U tests if statistically significant. A 5 % ($P < 0.05$) level of significance was adopted.

3 Results

3.1 Establishment of a rat osteoporotic model

As compared with sham-operated control, μCT images revealed that ovariectomy resulted in a significant decrease in the trabecular bone volume and density, remarkable increase in trabecular separation, disorganized trabecular microarchitecture, reduced cortical thickness and expanded marrow cavities (Fig. 2a, b, d, e). Structural parameters such as the BV/TV, Tb.N in the distal femur were significantly lower in OVX rats than in Sham rats ($P < 0.001$), whereas the Tb.Sp and P were significantly higher in OVX than in Sham rats ($P < 0.001$) (Table 2). The skeletal microarchitecture further deteriorated during this 2-month time frame. Histomorphometrical findings also proved the noticeable changes, such as plate-like trabecular pattern in Sham rats and rode-like trabecular pattern in OVX rats (Fig. 2c, f). Apart from the numerous osteoclasts lining around the trabecular surface (Fig. 6a, b), weakly positive Safranin O staining demonstrated that glycosaminoglycan was being degraded to make way for trabeculae formation, indicating that endochondral ossification is still present during osteoporosis development (Fig. 3A, a, E, e). Initial body weights (200 ± 10 g) were similar among all rats. After 2-month-induction, final body weight was significantly higher in OVX rats (233.81 ± 5.74 g) than in Sham rats (334.65 ± 10.18 g) ($P < 0.001$).

3.2 μCT analysis of osteogenesis

3D reconstruction of μCT images were performed as quantitative analysis of the morphology and mineralization of new bone formation within the defect. The analysis showed that drill control defects failed to regenerate appreciable bone tissue during a 4 week healing period, indicating that the critical size (non-self-healing ability) had been attained in the osteoporotic femur defects. Some minor mineralized tissue was visible for defects transplanted with pure silk and CaP/silk scaffolds, which was mainly restricted to the defect margins 2 weeks postsurgery. At 4 weeks, mineralized tissue bridging can be observed in the defect sites implanted with hybrid CaP/silk scaffolds, especially located to the peripheral side of cortical bone, significantly minimizing the defect region (Fig. 4). Similarly, as an indicator of the relative quantity of new bone formation, the value of BV/TV was the highest at both time points for the hybrid CaP/silk transplanted group, superior to the pure silk and drill control groups ($P < 0.05$; Fig. 5).

3.3 Histological observation and immunohistochemical assessment

Representative histological evidence of bone formation further supported the findings obtained by μCT analysis. No necrosis was present. In the drill control defects, a clear boundary of host bone with no evidence of bone formation within defect sites can be observed, with the exception of some sparsely distributed fibrous tissue (Fig. 4). A high percentage of osteoclasts surrounding and within the defect area was also observed (Figs. 6c, d, 7). Noticeably, osteoporotic bone marrow-like tissue with increased oval vacuolar adipocytes gradually filled the defect in the drill control group during the 4-week-healing period (Fig. 3B, b, F, f). The increased degradation of the remaining scaffolds caused the failure to maintain pore structural integrity in the hybrid CaP/silk scaffolds within the whole observation period, which is more remarkable than the pure silk group ($P < 0.05$; Fig. 8b),

accompanied with more increased bony ingrowth and larger quantity of stranded connective tissue mainly located in the center of the defect (Fig. 3).

A semi-quantitative scaling was used to compare the bone regeneration ability of our scaffolds (Table 1). Drill control defects had no or minimal bone formation at both time points, followed by small portion of bone formation in pure silk group, while statistically significant more amount of bone formation was observed in defects filled with hybrid CaP/silk scaffolds at 4 weeks ($P < 0.05$; Fig. 8A). Moreover, the positive Safranin O staining of cartilage matrix could be detected adjacent to the defect margin, demonstrating the occurrence of endochondral ossification at the periphery of the CaP/silk scaffold groups during the remodeling process by 4 weeks. Interestingly, the newly formed border bone tissue was quite histologically similar to the surrounding disorganized osteoporotic bone at both time points in the pure silk scaffold implants and at 2 weeks in the hybrid CaP/silk scaffold implants (Fig. 3C, c, D, d, G, g); however, at 4 weeks in the hybrid CaP/silk group, the bone structure improved and resembled sound trabeculea-like tissue (Fig. 3H, h).

Representative TRAP staining showed that osteoclasts in shuttle shape were lining around the osteoporotic trabecular surface in blank control group. In the drill control group, abundant mononuclear macrophages could be seen at the border of defect at 2 weeks, while mature and a significantly increased number of osteoclasts (nuclei of TRAP positive staining cells ≥3) were present by 4 weeks. After implanting pure silk, the osteoclast number was slightly decreased compared to drill control group. The highest number ($P < 0.01$) of osteoclasts co-existing with osteogenic cells could be found especially surrounding remnant scaffolds in defects filled with hybrid CaP/silk scaffolds at 2 weeks, indicating an activated bone remodeling process and dynamic degradation of the biomaterial. Subsequently, the number of osteoclasts decreased significantly ($P < 0.01$) at 4 weeks, suggesting a relatively high increase in bone formation when compared to bone resorption (Figs. 6, 7). As new bone formation should be accompanied by the markers that represent osteogenic progression, immunohistochemical analysis was performed to detect the expression of bone matrix proteins. A positively stronger expression of COL I and OPN over time could be observed within newly formed border bone in the hybrid CaP/silk scaffolds group when compared to pure silk group (Fig. 9).

4 Discussion

Osteoporotic defects are the most common complication of postmenopausal osteoporosis. Up to date, the prevention and therapeutic approaches of osteoporosis are mainly focused on medication treatment by inhibiting bone resorption (anticatabolic compounds), including bisphosphonates, calcitonin, and selective estrogen receptor modulators. In spite of further reversing loss of bone, these drugs do not stimulate new bone formation. Although PTH is the only FDA approved compound capable of stimulating new bone formation and preventing bone loss, the side effects such as hypercalcemia and hypercalciuria might be generated are safety threats [27]. Thus, it is necessary to develop new approaches to stimulate new bone regeneration and reverse bone loss following osteoporotic defects and fractures. The aim of the present study was to investigate the involved remodeling process of porous pure silk and CaP/silk composite scaffolds upon local implantation into critical sized

osteoporotic metaphyseal defects created in a rat distal femur model, and to compare the osteogenic efficiency during a 4 week healing period.

Although in vitro assays (e.g., cell cultures) might help to investigate the reaction of osteoporotic cells subsequent to diverse stimuli, they lack the effects of central control of bone turnover [28] and the feedback mechanisms involved in physical and pathological environment [29]. Laboratory ovariectomized rats are a FDA-recommended models [30] to represent the process (e.g., cortical and trabecular bone loss) that occurs in the presence of cytokines or hormonal factors, owning to the fast generation at low cost, easy and safe to handle, reliable reproducibility and their similarities to pathophysiological responses in postmenopausal cancellous bone loss [29, 31]. The skeletally immature rats achieved a low peak bone mass, which is considered to be a high risk factor for the development of human osteoporotic defects [32]. That's why we choose 3-month-old young adult rats as the animal model in our present research. In addition, as one of the weight-bearing bones, femur fractures often occur as a result of the weakening skeletal structure of untreated osteoporosis. Accordingly, ovariectomized rats with femoral head defects were chosen in our study which is readily available to assess the therapeutic effect of biomaterials in skeletal diseased conditions with a loading interference. The induction period of osteoporotic rat model varies, considering different ages and sites. Some researchers reported a period of 7-week–3-month to develop osteopenia in rat femur at age of 3 months [33–37]. Based on our results from μCT analysis and histological sections, and body weight measurement, after 2-month-induction, significant deterioration in the trabecular and cortical microstructure, expanded marrow cavities, earlier appearance and greater number of TRAP-positive cells, together with highly increased body weight demonstrated the successful establishment of an osteoporotic femur model. These results were consistent with previously reported findings [38, 39].

Silk has been used particularly as a suture material in the medical industry for centuries, prior to its widespread introduction as a synthetic polymers resulting from its unique mechanical properties [40]. As a well-known alternative to natural bone grafts, the use of CaP exhibits ideal properties such as non-toxic, resorbable, osteoconductive and 'intrinsic' osteoinductive of nano-sized particle [41]. 3D porous bioceramic-silk scaffolds are considered as a new branch of silk-based scaffolds for tissue regeneration. According to the results from our previous study, a more uniform and continuous pore network with enhanced mechanical strength was generated after incorporating CaP powders into porous silk scaffolds by freeze-drying methods, compared with that of pure ceramic scaffolds [19]. Recent studies showed that scaffolds with apatite coatings stimulate bone marrow stromal cells to heal critical size defects [42, 43]. To date, no research has compared the therapeutic effect of pure silk and hybrid CaP/silk scaffolds on osteoporotic defects.

The bone remodeling process in this osteoporotic defect model remained unclear. A recent study showed that an osseous femur defect created in osteoporotic mice resulted in bone healing primarily by intramembranous ossification [44]. In our study, trabecular-like bone tissue surrounded with abundant osteoblastic cells and traces of cartilage matrix were mainly located at the peripheral regions of defects filled with hybrid CaP/silk scaffolds. Control defects demonstrated an increase in oval vacuolar adipocytes, μCT analysis also supported

the accelerated mineralization of bone matrix within defects filled with hybrid CaP/silk scaffolds. This finding may suggest an activated remodeling process involving both intramembranous and endochondral ossification.

In osteoporosis, typically bone resorption outweighs bone formation [45]. In this study, we detected COL I, OPN and TRAP as markers for bone remodeling. COL I is regarded as the most abundant structural protein in bone matrix and is an early non-specific marker of osteoblastic differentiation during mineralization [46]. OPN is critical for the remodeling of mature bone by binding strongly to the CaP crystals and regulating the mineralization process [47]. The remarkable expression of COL I and OPN demonstrated that hybrid CaP/silk scaffolds can successfully promote bone matrix deposition and mineralization. The detection of many TRAP positive cells and significantly decreased amount of our CaP/silk scaffolds demonstrates the degradation of our scaffold in the early stages of defect healing. This observation is consistent with previous in vitro studies showing silk fibroin degradation by osteoclasts both from murine and human species [40, 41]. It can therefore be concluded that integration of CaP/silk scaffolds into osteoporotic defects seems to trigger a healthy balance between bone formation and bone resorption. The degradation of CaP/silk scaffolds is offset by a higher repair rate as demonstrated by the more pronounced increases in new bone formation.

Some likely factors contributing to the therapeutic effect of local transplanted hybrid CaP/silk scaffolds have previously been investigated. Firstly, the dissolution of calcium and phosphate ion from CaP containing composites not only enhances the bioactivity of materials [48] but also the proliferation, differentiation and mineralization of osteogenic cells [19]. A mild dissolution has been noted to provide a suitable calcium and phosphate ionic environment for bone formation, while a rapid dissolution may inhibit osteogenesis [49]. It has also been demonstrated that CaP-containing composites have strong protein adsorption capabilities for native bone morphogenetic proteins (BMPs) from body fluid, which then trigger CaP-induced bone formation [50]. Thirdly, the hybrid CaP/silk scaffolds we synthesized possess larger and more stable surface microstructures due to their improved pore structure and uniform distribution of CaP powders with 500 nm to 3 μm in diameter. It has been reported that scaffolds with micro-or nano-structures can provide a better osteogenic microenvironment for the attachment, proliferation and differentiation of MSCs into oteogenic cells[51], influence protein adsorption[52], and ease osseointegration of critical size bony defects [14]. Considering the consistent process of chronic skeletal deterioration in osteoporotic environment, a longer observation period can be followed to further investigate the changes within the defect sites.

In conclusion, compared with pure silk scaffolds as bone substitute biomaterials, 3D hybrid CaP/silk composite scaffolds are more useful by osseointegrating well after local implantation into critical sized osteoporotic defects. Findings from the present study demonstrate an activated remodeling process both through intramembranous and endochondral bone formation over skeletal deterioration. The accelerated mineralization and dynamic degradation of our scaffolds suggest the potential therapeutic efficacy of hybrid CaP/silk for the initial healing of osteoporotic defects.

Acknowledgments

Funding for this study was provided by research grants from the Natural Science Foundation of China (30700948) to Yufeng Zhang and (81170992) to Bin Shi, and the Fundamental Research Fund for the Central Universities (2012304274818) to Ning Cheng.

References

1. Tontonoz P, Pei LM. Fat's loss is bone's gain. J Clin Investig. 2004; 113:805–6. [PubMed: 15067310]
2. Rodan GA, Martin TJ. Therapeutic approaches to bone diseases. Science. 2000; 289:1508–14. [PubMed: 10968781]
3. Cooper C, Campion G, Melton LJ 3rd . Hip fractures in the elderly: a world-wide projection. Osteoporos Int. 1992; 2:285–9. [PubMed: 1421796]
4. Teitelbaum SL. Stem cells and osteoporosis therapy. Cell Stem Cell. 2010; 7:553–4. [PubMed: 21040895]
5. Moazzaz P, Gupta MC, Gilotra MM, Gilotra MN, Maitra S, et al. Estrogen-dependent actions of bone morphogenetic protein-7 on spine fusion in rats. Spine (Phila Pa 1976). 2005; 30:1706–11. [PubMed: 16094270]
6. Hao YJ, Zhang G, Wang YS, Qin L, Hung WY, et al. Changes of microstructure and mineralized tissue in the middle and late phase of osteoporotic fracture healing in rats. Bone. 2007; 41:631–8. [PubMed: 17652051]
7. Namkung-Matthai H, Appleyard R, Jansen J, Hao Lin J, Maastricht S, et al. Osteoporosis influences the early period of fracture healing in a rat osteoporotic model. Bone. 2001; 28:80–6. [PubMed: 11165946]
8. Silva BC, Bilezikian JP. New approaches to the treatment of osteoporosis. Annu Rev Med. 2011; 62:307–22. [PubMed: 21054170]
9. Kaplan D, Adams WW, Farmer B, Viney C. Silk—biology, structure, properties, and genetics. ACS Symp Ser. 1994; 544:2–16.
10. Kaplan DL, Wang YZ, Kim HJ, Vunjak-Novakovic G. Stem cell-based tissue engineering with silk biomaterials. Biomaterials. 2006; 27:6064–82. [PubMed: 16890988]
11. Kaplan DL, Vepari C. Silk as a biomaterial. Prog Polym Sci. 2007; 32:991–1007. [PubMed: 19543442]
12. Wang Y, Rudym DD, Walsh A, Abrahamsen L, Kim HJ, et al. In vivo degradation of three-dimensional silk fibroin scaffolds. Biomaterials. 2008; 29:3415–28. [PubMed: 18502501]
13. Meinel L, Hofmann S, Karageorgiou V, Kirker-Head C, McCool J, et al. The inflammatory responses to silk films in vitro and in vivo. Biomaterials. 2005; 26:147–55. [PubMed: 15207461]
14. Zhao J, Zhang Z, Wang S, Sun X, Zhang X, et al. Apatite-coated silk fibroin scaffolds to healing mandibular border defects in canines. Bone. 2009; 45:517–27. [PubMed: 19505603]
15. Costantino PD, Chaplin JM, Wolpoe ME, Catalano PJ, Sen C, et al. Applications of fast-setting hydroxyapatite cement: cranioplasty. Otolaryngol Head Neck Surg. 2000; 123:409–12. [PubMed: 11020176]
16. Giannoudis PV, Dinopoulos H, Tsiridis E. Bone substitutes: an update. Injury. 2005; 36(Suppl 3):S20–7. [PubMed: 16188545]
17. Goyenvalle E, Guyen NJ, Aguado E, Passuti N, Daculsi G. Bilayered calcium phosphate coating to promote osseointegration of a femoral stem prosthesis. J Mater Sci Mater Med. 2003; 14:219–27. [PubMed: 15348467]
18. Barrere F, van Blitterswijk CA, de Groot K. Bone regeneration: molecular and cellular interactions with calcium phosphate ceramics. Int J Nanomed. 2006; 1:317–32.
19. Zhang Y, Wu C, Friis T, Xiao Y. The osteogenic properties of CaP/silk composite scaffolds. Biomaterials. 2010; 31:2848–56. [PubMed: 20071025]
20. Sofia S, McCarthy MB, Gronowicz G, Kaplan DL. Functionalized silk-based biomaterials for bone formation. J Biomed Mater Res. 2001; 54:139–48. [PubMed: 11077413]

21. Lima I, Farias MLF, Percegoni N, Rosenthal D, de Assis JT, et al. Micro imaging analysis for osteoporosis assessment. Spectrochim Acta Part B At Spectrosc. 2010; 65:253–7.
22. Mankani MH, Kuznetsov SA, Avila NA, Kingman A, Robey PG. Bone formation in transplants of human bone marrow stromal cells and hydroxyapatite-tricalcium phosphate: prediction with quantitative CT in mice. Radiology. 2004; 230:369–76. [PubMed: 14752182]
23. Hutmacher DW, Sawyer AA, Song SJ, Susanto E, Chuan P, et al. The stimulation of healing within a rat calvarial defect by mPCL-TCP/collagen scaffolds loaded with rhBMP-2. Biomaterials. 2009; 30:2479–88. [PubMed: 19162318]
24. Ebneter A, Casson RJ, Wood JP, Chidlow G. Microglial activation in the visual pathway in experimental glaucoma: spatio-temporal characterization and correlation with axonal injury. Investig Ophthalmol Vis Sci. 2010; 51:6448–60. [PubMed: 20688732]
25. Fernandes JC, Wang H, Jreyssaty C, Benderdour M, Lavigne P, et al. Bone-protective effects of nonviral gene therapy with folate-chitosan DNA nanoparticle containing interleukin-1 receptor antagonist gene in rats with adjuvant-induced arthritis. Mol Ther. 2008; 16:1243–51. [PubMed: 18500247]
26. Kawaguchi H, Akune T, Ohba S, Kamekura S, Yamaguchi M, et al. PPAR gamma insufficiency enhances osteogenesis through osteoblast formation from bone marrow progenitors. J Clin Investig. 2004; 113:846–55. [PubMed: 15067317]
27. Khosla S, Westendorf JJ, Oursler MJ. Building bone to reverse osteoporosis and repair fractures. J Clin Investig. 2008; 118: 421–8. [PubMed: 18246192]
28. Haberland M, Schilling AF, Rueger JM, Amling M. Brain and bone: central regulation of bone mass. A new paradigm in skeletal biology. J Bone Joint Surg Am. 2001; 83-A:1871–6. [PubMed: 11741068]
29. Egermann M, Goldhahn J, Schneider E. Animal models for fracture treatment in osteoporosis. Osteoporos Int. 2005; 16(Suppl 2):S129–38. [PubMed: 15750681]
30. Bonjour JP, Ammann P, Rizzoli R. Importance of preclinical studies in the development of drugs for treatment of osteoporosis: a review related to the 1998 WHO guidelines. Osteoporos Int. 1999; 9:379–93. [PubMed: 10550456]
31. Turner AS. Animal models of osteoporosis–necessity and limitations. Eur Cell Mater. 2001; 1:66–81. [PubMed: 14562261]
32. Lelovas PP, Xanthos TT, Thoma SE, Lyritis GP, Dontas IA. The laboratory rat as an animal model for osteoporosis research. Comp Med. 2008; 58:424–30. [PubMed: 19004367]
33. Boyd D, Carroll G, Towler MR, Freeman C, Farthing P, et al. Preliminary investigation of novel bone graft substitutes based on strontium-calcium-zinc-silicate glasses. J Mater Sci Mater Med. 2009; 20:413–20. [PubMed: 18839286]
34. Bossini PS, Renno AC, Ribeiro DA, Fangel R, Peitl O, et al. Biosilicate(R) and low-level laser therapy improve bone repair in osteoporotic rats. J Tissue Eng Regen Med. 2011; 5:229–37. [PubMed: 20925130]
35. Li Y, Li Q, Zhu S, Luo E, Li J, et al. The effect of strontium-substituted hydroxyapatite coating on implant fixation in ovariectomized rats. Biomaterials. 2010; 31:9006–14. [PubMed: 20800275]
36. Kumar A, Gupta GK, Khedgikar V, Gautam J, Kushwaha P, et al. In vivo efficacy studies of layer-by-layer nano-matrix bearing kaempferol for the conditions of osteoporosis: a study in ovariectomized rat model. Eur J Pharm Biopharm. 2012; 82:508–17. [PubMed: 22926146]
37. Zhang Y, Cheng N, Miron R, Shi B, Cheng X. Delivery of PDGF-B and BMP-7 by mesoporous bioglass/silk fibrin scaffolds for the repair of osteoporotic defects. Biomaterials. 2012; 33:6698–708. [PubMed: 22763224]
38. Ikeda T, Yamaguchi A, Yokose S, Nagai Y, Yamato H, et al. Changes in biological activity of bone cells in ovariectomized rats revealed by in situ hybridization. J Bone Miner Res. 1996; 11:780–8. [PubMed: 8725175]
39. Jiang JM, Sacco SM, Ward WE. Ovariectomy-induced hyperphagia does not modulate bone mineral density or bone strength in rats. J Nutr. 2008; 138:2106–10. [PubMed: 18936205]
40. Kaplan DL, Altman GH, Diaz F, Jakuba C, Calabro T, et al. Silk-based biomaterials. Biomaterials. 2003; 24:401–16. [PubMed: 12423595]

41. Barbieri D, Renard AJS, de Bruijn JD, Yuan H. Heterotopic bone formation by nano-apatite containing poly(D,L-Lactide) composites. Eur Cells Mater. 2010; 19:252–61.

42. den Boer FC, Wippermann BW, Blokhuis TJ, Patka P, Bakker FC, et al. Healing of segmental bone defects with granular porous hydroxyapatite augmented with recombinant human osteogenic protein-1 or autologous bone marrow. J Orthop Res. 2003; 21:521–8. [PubMed: 12706026]

43. Yang H, Wang G, Li M, Lu S, Chen X, et al. The use of silk fibroin/hydroxyapatite composite co-cultured with rabbit bone-marrow stromal cells in the healing of a segmental bone defect. J Bone Joint Surg Br. 2010; 92B:320–5.

44. He YX, Zhang G, Pan XH, Liu Z, Zheng LZ, et al. Impaired bone healing pattern in mice with ovariectomy-induced osteoporosis: a drill-hole defect model. Bone. 2011; 48:1388–400. [PubMed: 21421090]

45. Ramprasath VR, Shanthi P, Sachdanandam P. Curative effect of Semecarpus anacardium Linn. nut milk extract against adjuvant arthritis—with special reference to bone metabolism. Chem Biol Interact. 2006; 160:183–92. [PubMed: 16513099]

46. Cowles EA, DeRome ME, Pastizzo G, Brailey LL, Gronowicz GA. Mineralization and the expression of matrix proteins during in vivo bone development. Calcif Tissue Int. 1998; 62:74–82. [PubMed: 9405737]

47. Denhardt DT, Noda M, O'Regan AW, Pavlin D, Berman JS. Osteopontin as a means to cope with environmental insults: regulation of inflammation, tissue remodeling, and cell survival. J Clin Investig. 2001; 107:1055–61. [PubMed: 11342566]

48. van Blitterswijk CA, Habibovic P, Yuan HP, van der Valk CM, Meijer G, et al. 3D microenvironment as essential element for osteoinduction by biomaterials. Biomaterials. 2005; 26:3565–75. [PubMed: 15621247]

49. Yuan H, Yang Z, Li Y, Zhang X, De Bruijn JD, et al. Osteoinduction by calcium phosphate biomaterials. J Mater Sci Mater Med. 1998; 9:723–6. [PubMed: 15348929]

50. Yuan H, Zou P, Yang Z, Zhang X, De Bruijn JD, et al. Bone morphogenetic protein and ceramic-induced osteogenesis. J Mater Sci Mater Med. 1998; 9:717–21. [PubMed: 15348928]

51. Dalby MJ, Gadegaard N, Tare R, Andar A, Riehle MO, et al. The control of human mesenchymal cell differentiation using nano-scale symmetry and disorder. Nat Mater. 2007; 6:997–1003. [PubMed: 17891143]

52. Zhu XD, Fan HS, Xiao YM, Li DX, Zhang HJ, et al. Effect of surface structure on protein adsorption to biphasic calcium-phosphate ceramics in vitro and in vivo. Acta Biomater. 2009; 5:1311–8. [PubMed: 19121984]

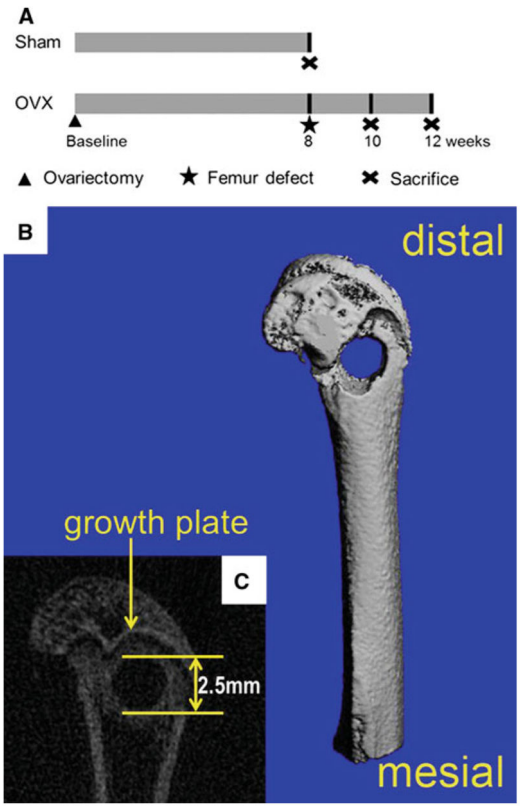

Fig. 1.

Schematic diagram indicating the time points of surgery on Sham and OVX rats. 2 month after ovariectomy, OVX rats were assigned to confirm the establishment of osteoporotic model, using Sham rats as control. Meanwhile, femur defect drilling was performed in OVX rats, followed by implanting the scaffolds. After 2 and 4 weeks healing periods, OVX rats were sacrificed and the femur specimens were removed for assessments (**a**). Schematic presentation of the dimension and position of femur defect using μCT images (**b**, **c**)

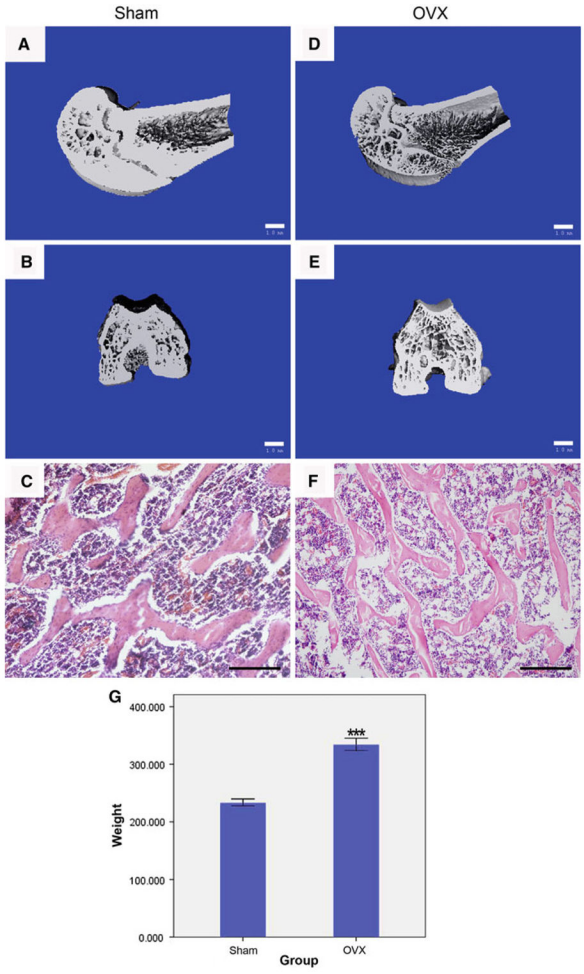

Fig. 2.

Establishment of rat osteoporotic model. 3D-μCT images of distal femur from Sham rats (**a**, **b**) and OVX rats (**d**, **e**; *bar* = 1 mm). H&E staining of subchondral trabecular bone showed a plate-like trabecular pattern in Sham group (**c**) and deterioration into rode-like pattern in OVX rats (**f**, **g**; bar = 200 μm). The body weight of OVX rats was significantly higher than those in Sham control

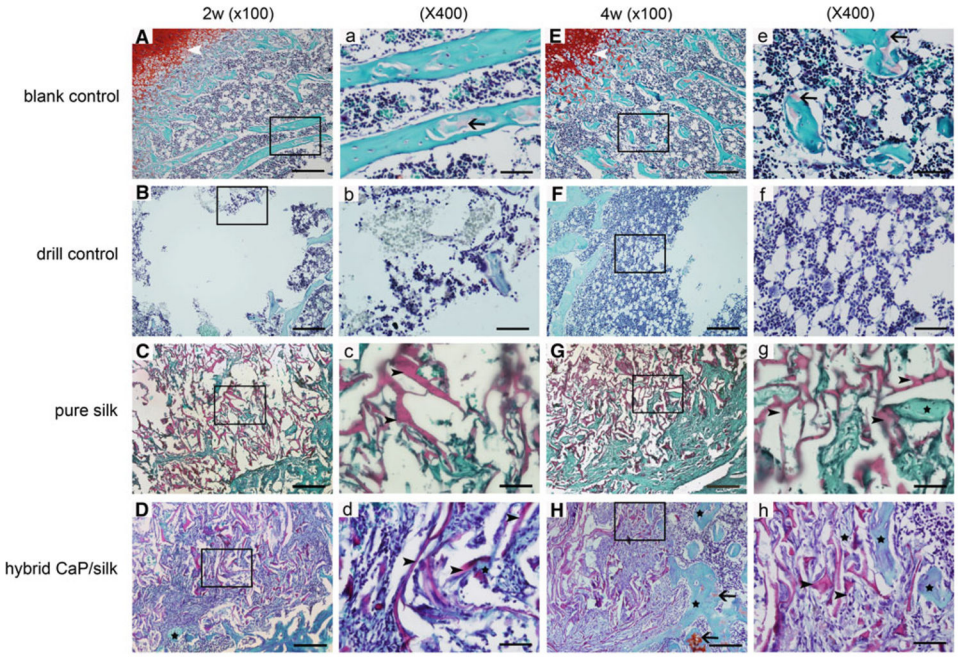

Fig. 3.

Representative Safranin O staining of subchondral bone formation 2 and 4 weeks after surgery at low (×100; *bar* = 200 μm) and high (×400; *bar* = 50 μm) magnification. Weakly positive staining (*black arrow*) demonstrated the presence of cartilage matrix in the blank control group during osteoporosis development (**A**, **a**, **E**, **e**). Osteoporotic bone marrow-like tissue with increased oval vacuolar adipocytes gradually filled the defect in the drill control group (**B**, **b**, **F**, **f**). The degradation of remaining scaffolds (*black arrow head*) were accompanied with increased bony ingrowth (*black star*) and stranded connective tissue surrounded by osteoblastic cells in the pure silk and hybrid CaP/silk scaffolds group (**C**–**D**, **c**–**d**, **G**–**H**, **g**–**h**)

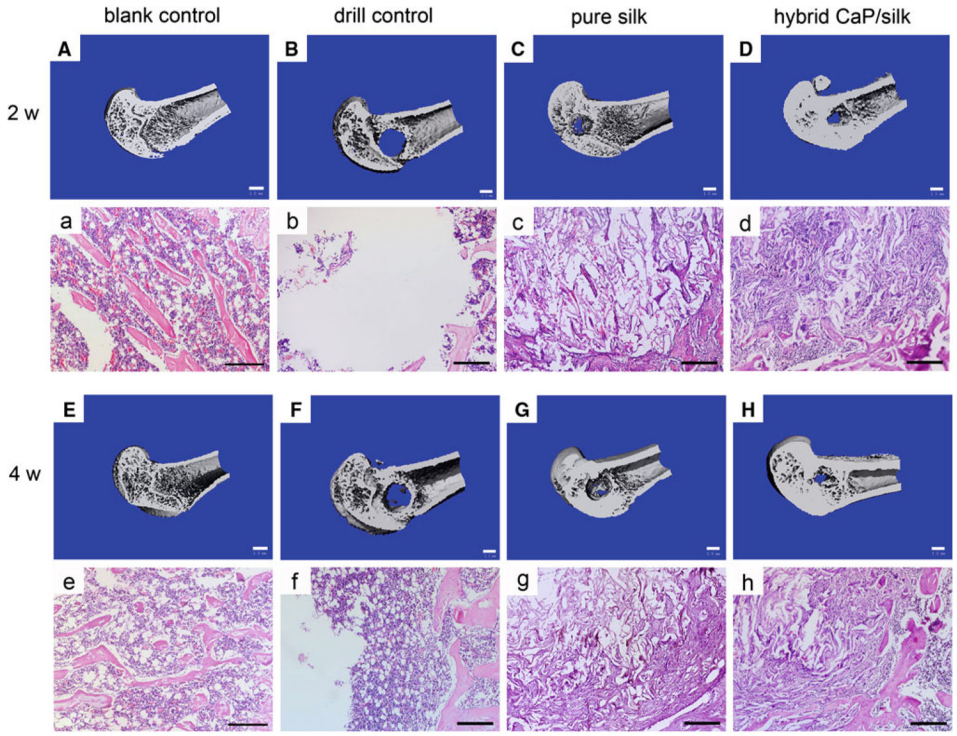

Fig. 4.

3D reconstruction of distal femur represented mineralized bone formation within defects in the blank control group, drill control group, pure silk scaffolds group and the hybrid CaP/silk scaffolds group (**A**–**H**; *bar* = 1 mm). H&E staining revealed new bone matrix deposition within defects in the above mentioned groups (**a**–**h**; *bar* = 200 μm)

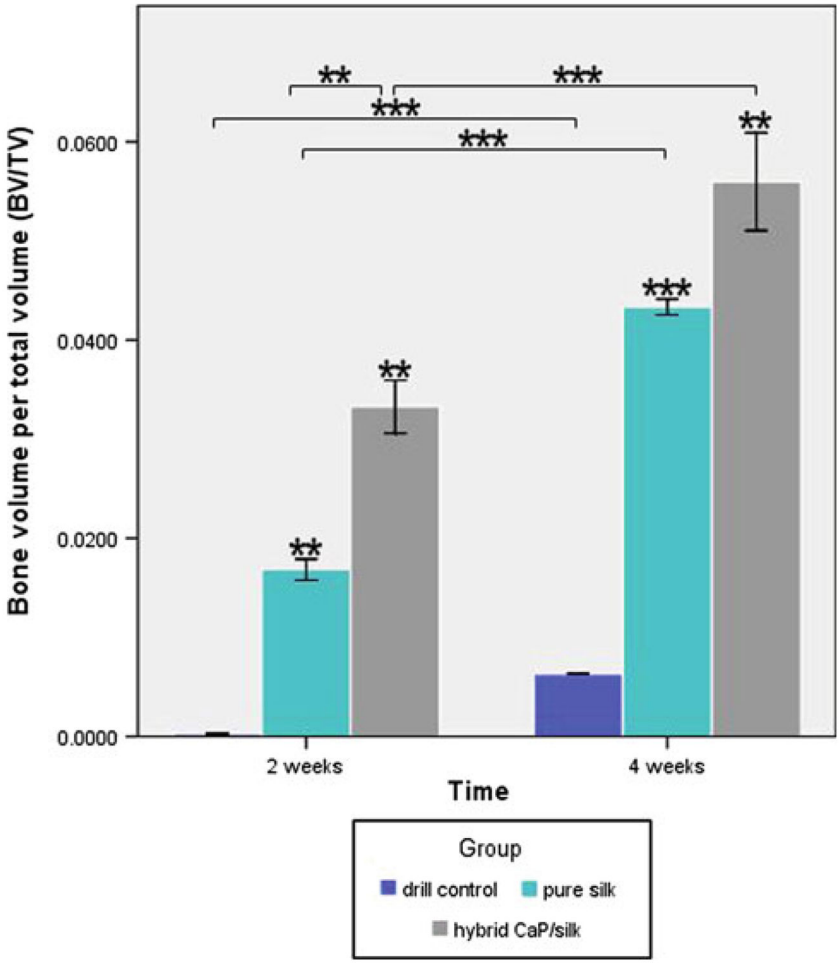

Fig. 5.

Quantitative comparision of BV/TV among the drill control, pure silk and hybrid CaP/silk groups at two time points by two-tail student *t* test: **P* < 0.05, ***P* < 0.01, ****P* < 0.001

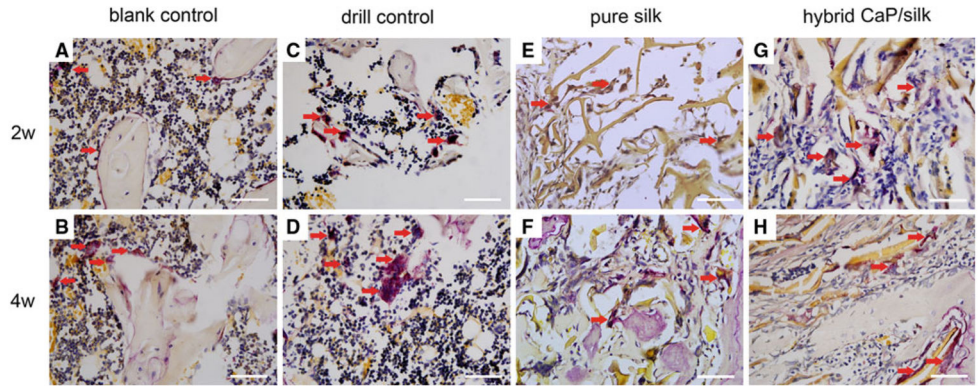

Fig. 6.

Representative TRAP staining showed that osteoclasts (*red arrow*) in shuttle shape were lining around osteoporotic trabecular surface in blank control group (**a**, **b**), abundant mononuclear macrophages gradually fused into mature osteoclasts within defect in drill control group (**c**, **d**), osteoclasts co-existed with osteogenic cells could be found especially surrounding remaining scaffolds in the pure silk and hybrid CaP/silk scaffolds group (**e**–**h**). (×400; *bar* = 50 μm) (Color figure online)

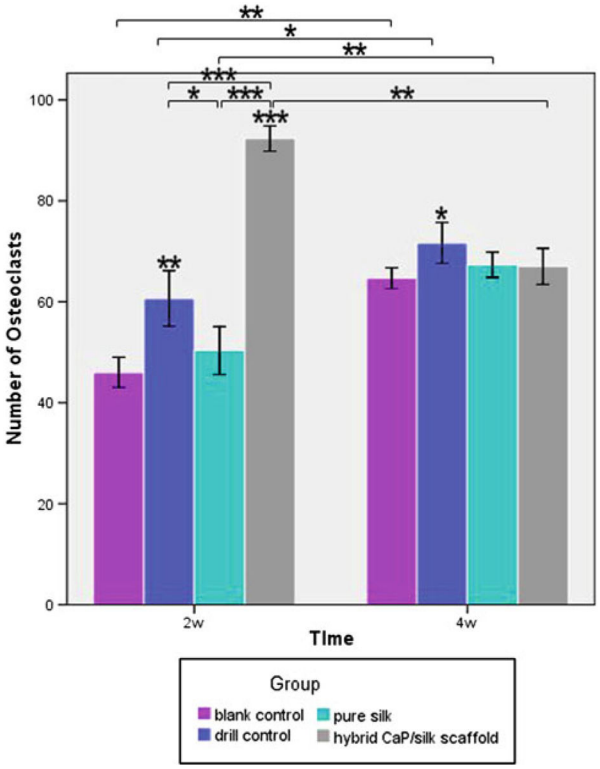

Fig. 7.

The number of TRAP-positive osteoclasts counted at low magnification (×100) within defect sites at both time points. *$P < 0.05$, **$P < 0.01$, ***$P < 0.001$

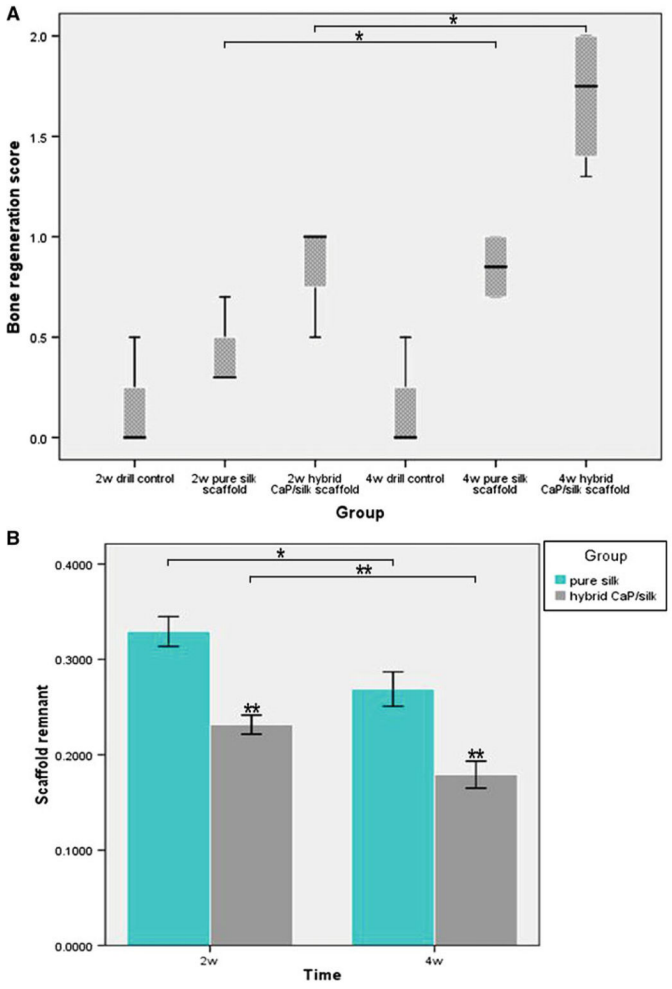

Fig. 8.

a Semi-quantitative scores of bone regeneration within femur defect are present as box plots. The box represents the 25 and 75 percentiles and the horizontal line in the box represents median value. Lines outside the box represent the spread of values. **b** Quantitative comparision of scaffold remnant fraction in hybrid CaP/silk group at two time point by two-tail student *t* test. (Scaffold remnant equals to the area of silk scaffolds compared to total area) $*P < 0.05$, $**P < 0.01$

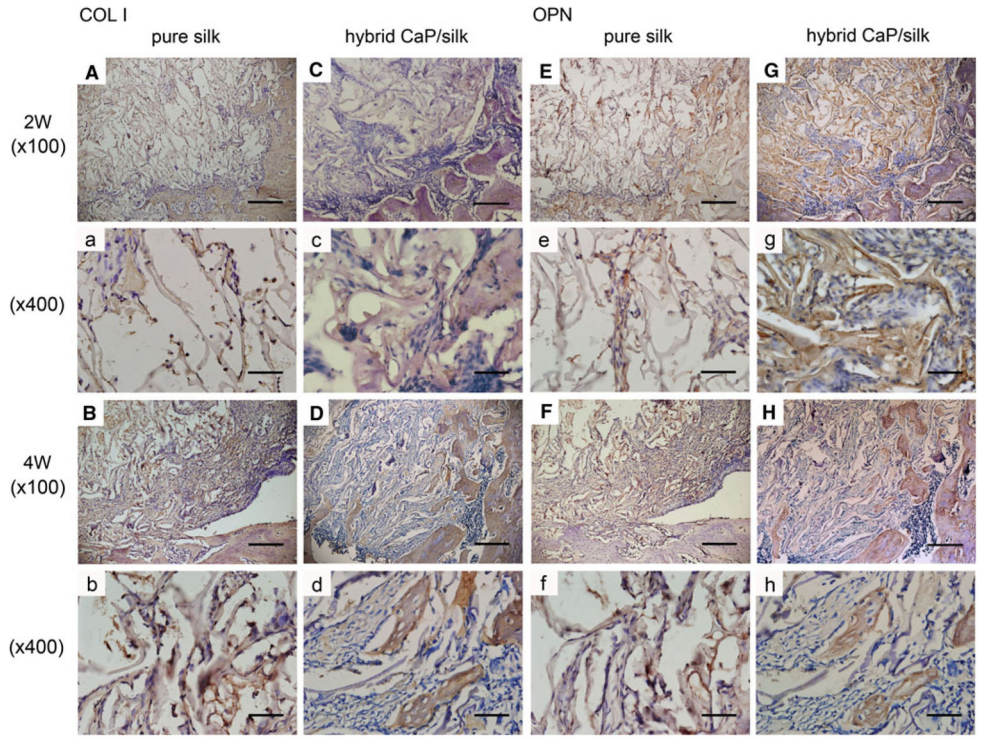

Fig. 9.

The expression of COL I and OPN were positively stronger in the hybrid CaP/silk scaffolds group than in the pure silk scaffolds group. An increased expression could be detected in newly formed border bone compared to that located centrally. High magnification (×100), *bar* = 200 μm; low magnification (×400), *bar* = 50 μm)

Table 1

Semiquantitative scale for evaluation of bone regeneration

Score	Extent of new bone in defect
0	No bone formation
1	Minimal bone formation (only very small portion in the defect)
2	Low bone formation (less than one-forth of the defect)
3	Moderate bone formation (less than one-half and more than one-forth of the defect)
4	Abundant bone formation (more than one-half of the defect)

Table 2

μCT analysis of bone volume per total volume (BV/TV), trabecular number (Th.N), trabecular thickness (Tb.Th), trabecular separation (Th.Sp) and porosity (P) in intact distal femurs from Sham, OVX, 2w blank control and 4w blank control rats

	Sham	OVX	OVX + 2w	OVX + 4w
BV/TV	0.423 ± 0.019	0.221 ± 0.009 ***	0.152 ± 0.021***	0.026 ± 0.001***
Tb.N	4.727 ± 0.060	4.055 ± 0.028 ***	2.366 ± 0.057 ***	2.236 ± 0.159***
Tb.Th	0.207 ± 0.028	0.117 ± 0.002	0.107 ± 0.003	0.069 ± 0.001*
Tb.Sp	0.205 ± 0.004	0.428 ± 0.002 ***	0.445 ± 0.014 ***	0.375 ± 0.103***
P	0.577 ± 0.019	0.779 ± 0.009 ***	0.848 ± 0.021 ***	0.955 ± 0.016***

* $P < 0.05$ and *** $P < 0.001$ versus the corresponding Sham group